

Interband second-harmonic generation in $\text{Zn}_{1-x}\text{Cd}_x\text{Se}/\text{ZnSe}$ strained quantum wells

Vittorio Pellegrini, Andrea Parlangei, Marco Börger, Rosen D. Atanasov,* and Fabio Beltram
Scuola Normale Superiore, Piazza dei Cavalieri 7, I-56126 Pisa, Italy

Lia Vanzetti[†] and Alfonso Franciosi[‡]

Laboratorio Tecnologie Avanzate Superfici e Catalisi dell'Istituto Nazionale per la Fisica della Materia, I-34012 Trieste, Italy

(Received 30 May 1995)

We report continuous-wave interband second-harmonic generation (SHG) at 460–480 nm in strained $\text{Zn}_{1-x}\text{Cd}_x\text{Se}/\text{ZnSe}$ asymmetric quantum wells grown by molecular-beam epitaxy. The dependence of the SHG intensity on the fundamental frequency allowed us to identify the individual quantum-well exciton resonances in the second-harmonic signal. The strongest SHG was found to be associated with light-hole exciton transitions. Numerical calculations of the SHG intensity that take into account exciton and continuum states yielded predictions in remarkable agreement with experiment.

The nonlinear optical properties of semiconductor quantum wells have a number of possible applications in the field of information technology. The study of excitonic third-order optical nonlinearities,^{1–3} for example, is leading to the implementation of practical devices.^{4,5} Several theoretical and experimental reports on second-order nonlinear effects in semiconductor heterostructures have also been published.^{6–9} Among the many interesting and potentially useful effects, second-harmonic generation (SHG) has been the subject of intense experimental investigation especially in relation to intravalence band^{10,11} and intraconduction band^{9,12} transitions. Symmetry considerations indicate that SHG and, in general, second-order nonlinear effects should be enhanced in noncentrosymmetric structures, and intersubband SHG has been demonstrated in several asymmetric quantum-well (AQW) heterostructures.

Interband SHG include excitonic effects and can therefore be considered as a potentially important probe of the fundamental optical properties in the near-band-gap region. The comparatively small amount of information available on interband SHG (Refs. 13 and 14) reflects primarily the fact that interband SHG intensity in AQW's is expected to be comparable with that observed in bulk materials, owing to the difficulty of achieving a double resonance enhancement.¹⁵ Appreciable SH conversion efficiency, however, has been recently achieved exploiting resonant cavities¹⁶ and quasi-phase matching (QPM) conditions. In this paper we demonstrate a different approach and report SHG from multiple asymmetric $\text{Zn}_{1-x}\text{Cd}_x\text{Se}/\text{ZnSe}$ coupled quantum wells (ACQW's) with intensity well above that achieved in bulk ZnSe.

We conducted studies of SHG in reflection geometry from strained $\text{Zn}_{1-x}\text{Cd}_x\text{Se}/\text{ZnSe}$ ACQW's and from reference ZnSe samples with the twofold purpose of investigating the contribution of different exciton states to the second-order process, and estimating the effect of the ACQW potential relative to that of the surface and bulk material in determining SHG. Our results show that a threefold enhancement of SHG can be achieved in the presence of the ACQW potential even without a resonant cavity or QPM conditions, and emphasize the role of the light-hole (lh) exciton states in SHG.

These lh exciton states are confined mainly by the electron-hole Coulomb interaction as opposed to the valence band discontinuity,^{17,18} and the set of consistent exciton parameters that we have recently obtained from the optical and electrical properties of $\text{Zn}_{1-x}\text{Cd}_x\text{Se}/\text{ZnSe}$ quantum wells^{17,19} were found to be essential to model the ACQW heterostructures and optimize their nonlinear response.

The samples studied in this work were grown by solid source molecular-beam epitaxy (MBE) on GaAs(001) n^+ substrates, utilizing a facility with interconnected MBE chambers for the growth of II-VI and III-V materials. A 0.5 μm thick n -type GaAs(001) 2×4 epitaxial layer was first grown at 580 °C on GaAs(001) wafers in the III-V MBE growth chamber. On such substrates, a 0.5 μm thick undoped ZnSe buffer layer was grown at 290 °C in the II-VI MBE chamber. The ACQW sample was composed of ten asymmetric coupled quantum wells separated by 10 nm ZnSe barriers. Each ACQW consisted of a 3.5 nm thick $\text{Zn}_{0.74}\text{Cd}_{0.26}\text{Se}$ well separated from a thinner (2 nm) well of the same composition by a 1.5 nm ZnSe barrier. With such layer thicknesses, the ZnSe buffer was completely relaxed relative to the GaAs substrate, the ACQW's grew pseudomorphically on the ZnSe buffer, and the $\text{Zn}_{0.74}\text{Cd}_{0.26}\text{Se}$ wells were under a substantial compressive strain because of the lattice mismatch ($\sim 2\%$) with ZnSe. Wells and barriers were grown at 250 °C with 30 s growth interruption at each interface. For comparison, SHG studies were also performed on a 0.5 μm thick undoped ZnSe buffer layer grown in identical conditions as the ACQW sample.

A schematic illustration of the electronic structure of the asymmetric quantum well is depicted in the leftmost inset of Fig. 1, where electron and heavy-hole confining potentials are shown using the experimental band offsets.¹⁹ The $e1$, $e2$ electron and $hh1$, $hh2$ heavy-hole levels, and the corresponding envelope functions are also shown, as calculated using a two-band model in the envelope-function approximation.¹⁷

The samples were attached to the cold finger of a helium-gas cryocooler. Lattice temperature was monitored with a calibrated Si-diode thermometer mounted next to the sample. In order to detect local heating effects we systematically ana-

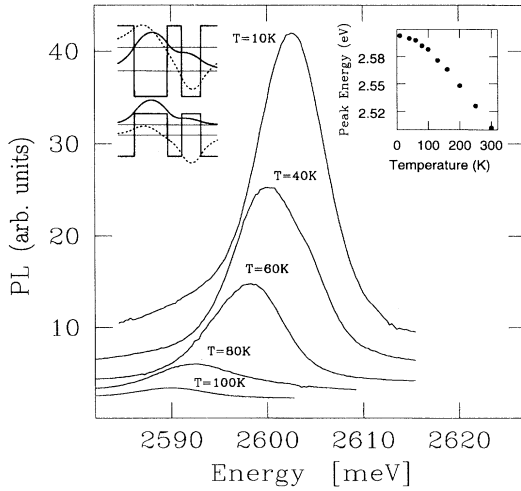


FIG. 1. Photoluminescence spectra of the sample at several temperatures between 10 K and 100 K. The spectra were excited by the 458 nm line of an Ar^+ laser with 1 mW incident power. In the right inset the observed hh1-e1 $1S$ -exciton peak energy is plotted as a function of the temperature. Electron and heavy-hole confining potentials are sketched in the left inset together with the $e1$, $e2$ electron and hh1 , hh2 heavy-hole levels and the corresponding envelope functions.

lyzed the energy of the photoluminescence (PL) exciton peak. PL spectra of the sample were recorded at several temperatures between 10 K and 100 K, using the 458 nm line of an Ar^+ laser with 1 mW incident power for the excitation. Representative PL spectra are shown in Fig. 1. The rightmost inset of Fig. 1 displays the resulting temperature dependence of the hh1-e1 $1S$ exciton peak energy.

The SH light was excited by a cw argon-laser pumped Ti:sapphire ring laser tunable in the 1270–1350 meV range. The exciting radiation was incident at 45° onto the sample, with an intensity of a few tens of kW/cm^2 (total incident power ≤ 300 mW). The SH signal radiated along the reflected beam was spectrally resolved by a 1 m Jobin-Yvon double monochromator and detected by conventional photon-counting techniques.

In the upper panel of Fig. 2 we plot the SH emission intensity at $2\hbar\omega$ from the ACQW's, as a function of the fundamental photon energy $\hbar\omega$, with $\hbar\omega$ in the 1280–1360 meV range. The data were obtained for p -polarized (in the plane of incidence) incident light and a cold-finger temperature of 10 K. The signal was normalized to that of a bulk standard in order to emphasize the ACQW's spectral contribution and correct for the spectral response of the laser. The marked variations in SHG efficiency as a function of the fundamental frequency depicted in the upper panel of Fig. 2 are a clear manifestation of the contributions of the individual excitonic resonances to the SHG signal. The PL spectra of Fig. 1 allow us to identify the first structure in the upper panel of Fig. 2 with the hh1-e1 resonance and suggests a local heating of the sample at lattice temperatures up to 80–90 K (see rightmost inset of Fig. 1). Local heating can be linked to free-carrier and two-photon absorption in the n -doped GaAs substrate. This is supported by the observation of a corresponding redshift of the PL peak when the

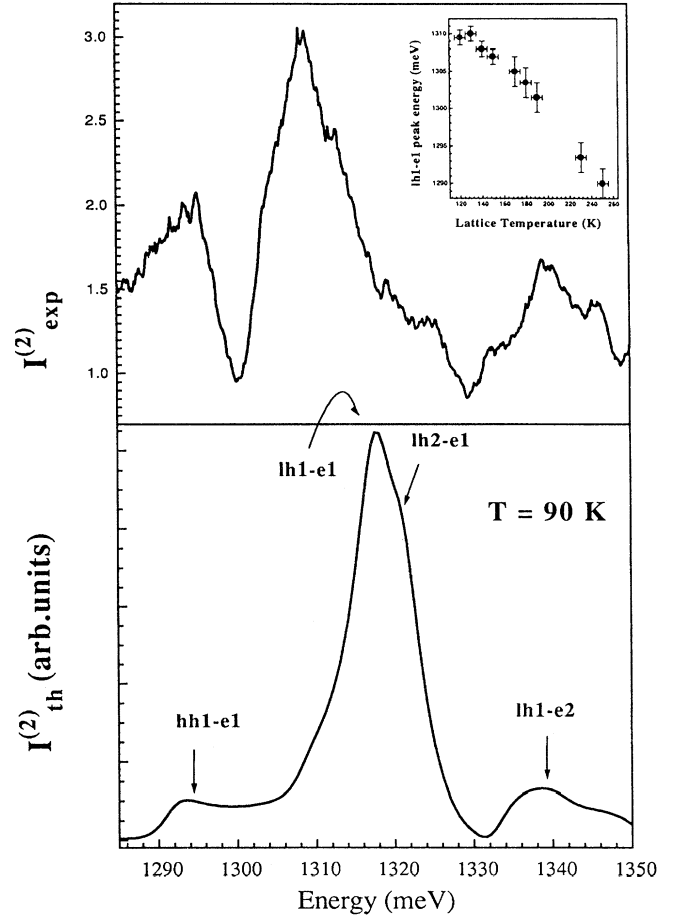


FIG. 2. (Upper panel) Experimental second-harmonic (SH) intensity ($I_{\text{exp}}^{(2)}$) as a function of the incident photon energy. The spectrum is obtained after normalization with respect to the SH emission of a reference ZnSe bulk sample. In the inset the observed dependence of the lh1-e1 $1s$ exciton peak on the local temperature of the sample is also shown. (Lower panel) Calculated SH intensity ($I_{\text{th}}^{(2)}$). The lattice temperature was set to 90 K. All material parameters are taken from Refs. 17 and 19.

emitting sample area is also irradiated by the focused Ti:sapphire. The dominant structure in the upper panel of Fig. 2 corresponds to the light-hole exciton resonance (see lower panel). Its temperature dependence is reported in the inset. The effect of the presence of the ACQW's is to enhance the SH emission intensity $I_{\text{ACQW}}^{(2)}$ and therefore the SHG efficiency at the light-hole exciton resonance by a factor of about 3 relative to the emission intensity $I_b^{(2)}$ from a similar sample without ACQW's, including therefore only the sum of the surface and bulk contributions.

To the best of our knowledge the surface and bulk relative contributions have not been experimentally determined in this system. The second-order susceptibility of the bulk in this spectral range, however, can be estimated from Ref. 20 to be $\chi_{(b)}^2 = 5 \times 10^{-11}$ m/V. By measuring the dependence of the surface plus bulk contribution on the polarization of the incident radiation, we can identify a lower limit of about 5 for the surface/bulk relative contribution. This estimate is

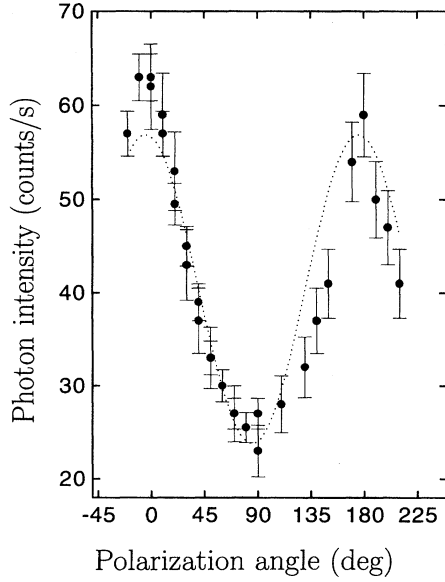


FIG. 3. Dependence of the second-harmonic signal at 2617 meV (incident photon energy 1308.5 meV) on the polarization of the fundamental light at a sample holder temperature $T=10$ K. The maxima correspond to incident light polarized in the plane of incidence (p polarization). Dashed lines are given by a best-fit procedure with the expected $\cos^2(\theta)$ dependence.

consistent with the known results in III-V zinc blende systems.¹⁴ If we use this value and the results for the bulk, we can write $\chi_{\text{ACQW}}^{(2)} \approx 10^{-10}$ m/V.

The polarization dependence of the SH signal was investigated by rotating the polarization of the fundamental beam and analyzing the polarization of the SH signal. In Fig. 3 we plot the total SH emission intensity at the light-hole exciton resonance (SH at 2617 meV and fundamental at 1308.5 meV) as a function of the exciting beam polarization, for a cold-finger temperature of 10 K. The minimum signal was obtained for s -polarized incident radiation. In these conditions, the residual SHG can be associated to the bulk and to the $\chi_{\text{zxx}}^{(2)}$ contribution of the surface (the $\chi_{\text{zxx}}^{(2)}$ contribution of the ACQW's is nonresonant in the half-gap region and therefore is negligible). Maximum SHG was observed for p polarization of the incident radiation. The overall polarization dependence of the SH intensity displays the expected $\cos^2(\theta)$ dependence (see dashed line in Fig. 3, as derived from a least squares fitting procedure).

To unambiguously identify the contribution of the individual excitonic resonances to the SH spectrum, we calculated the nonzero components of the second-order susceptibility $\chi^{(2)}$ for SHG using the density matrix approach in the electric-dipole approximation.⁶ In the mean-field approximation the second-order polarization $\mathbf{P}^{(2)}$ is given by

$$P_i^{(2)}(2\omega) = \frac{1}{2} \chi_{ijk}^{(2)} E_j(\omega) E_k(\omega), \quad (1)$$

where \mathbf{E} is the average QW electric field. Neglecting the small linear terms in the Luttinger Hamiltonian describing the heterostructure, O_h and C_{4v} are the point groups of the

bulk and of the ACQW, respectively. In this approximation there are only three independent nonzero $\chi^{(2)}$ elements and (1) takes the form²⁰

$$\begin{aligned} P_x^{(2)} &= \chi_{\text{xxz}}^{(2)} E_x E_z; & P_y^{(2)} &= \chi_{\text{xxz}}^{(2)} E_y E_z; \\ P_z^{(2)} &= \frac{1}{2} [\chi_{\text{zxx}}^{(2)} (E_x^2 + E_y^2) + \chi_{\text{zzz}}^{(2)} E_z^2]. \end{aligned} \quad (2)$$

We have used a two-band model in the envelope-function approximation in order to calculate the electron and hole continuum states.²¹ The same approach yielded the exciton eigenstates and the dipole matrix elements entering the evaluation of the second-order susceptibility. We took into account four different types of transitions: (1) ground-state-continuum, (2) ground-state-exciton, (3) continuum-continuum, and (4) exciton-exciton. Following the same theoretical approach we evaluated also the linear dielectric constant ϵ_{ACQW} that has to be included in the calculation of the reflected intensity.

In the case of a nonlinear slab (i.e., the ACQW's) with thickness d small compared to the fundamental wavelength, embedded between two linear dielectrics (air and the ZnSe buffer layer), the reflected SH electric field generated by a p -polarized fundamental beam is p polarized, and its amplitude is given by²²

$$\begin{aligned} E_p^R &= -i4\pi P^{(2)} \omega d c^{-1} [(\epsilon_{\text{ZnSe}} / \epsilon_{\text{ACQW}})^{1/2} \sin(\theta_{\text{ACQW}}) \\ &\quad \times \cos(\theta_s + \alpha) + \cos(\theta_{\text{ZnSe}}) \sin(\theta_s + \alpha)] \\ &\quad \times [\epsilon_{\text{ZnSe}}^{1/2} \cos(\theta_{\text{air}}) + \cos(\theta_{\text{ZnSe}})]^{-1}, \end{aligned} \quad (3)$$

where θ_{ACQW} and θ_s are the angles between the z axis and the second-harmonic and fundamental propagation directions, in the ACQW's region, respectively, θ_{air} and θ_{ZnSe} are the angle between the z axis and the fundamental propagation direction in air and in the ZnSe buffer layer, α is the angle between the nonlinear polarization and the fundamental wave, and $\epsilon_{\text{ZnSe}} = 8.7$. In particular, ϵ_{ACQW} can be calculated using the relation

$$\epsilon_{\text{ACQW}} = \frac{\sin^2(\theta_{\text{ACQW}})}{\epsilon_{\parallel}(2\omega)} + \frac{\cos^2(\theta_{\text{ACQW}})}{\epsilon_z(2\omega)}, \quad (4)$$

where $\epsilon_{\parallel,z}$ are the components of the linear dielectric constant of the ACQW in the plane of the wells and along the growth direction.²³

The SH reflected intensity is then computed using (2)–(4) by $I^{(2)}(2\omega) \propto c |E_p^R|^2$.

In the lower panel of Fig. 2 we plot the spectral dependence of the SH intensity calculated by means of Eqs. (2) and (3) at a lattice temperature of 90 K. There is remarkable agreement between the calculated and the experimental spectrum in Fig. 2, both exhibiting three main resonances, with a dominant feature corresponding to the light-hole resonance. The different attributions based on the calculations are marked in the lower panel of Fig. 2 near each spectral feature.

One of the most impressive features of both the experimental and the theoretical spectrum is the strongly enhanced lh1-e1 1S-exciton SH emission relative to that of the hh1-e1 1S exciton. Our calculations show that this primarily reflects the strain-induced delocalization of the light hole. We

found that the lh-*e* bonding decreases with increased light-hole delocalization, leading to an enhancement of anharmonicity and nonlinearities. The light-hole exciton dipole momenta entering the evaluation of the $\chi^{(2)}$ components are correspondingly enhanced, and more than compensate for the lower light-hole exciton oscillator strength.²⁵

In conclusion, by utilizing $\text{Zn}_{1-x}\text{Cd}_x\text{Se}/\text{ZnSe}$ multiple asymmetric quantum wells we were able to obtain enhanced interband SHG, and probe in detail the contribution of the individual excitonic resonances to the spectral dependence of SHG. We found that the lh1-*e*1 1*S*-exciton SH emission is

strongly enhanced relative to that of the hh1-*e*1 1*S* exciton as a result of the strain-induced delocalization of the light hole. Interband SHG has been shown to be a sensitive probe of semiconductor optical properties in the near-band-gap region.

We wish to thank Franco Bassani, Giuseppe La Rocca, and Alessandro Tredicucci for useful discussions, and Massimo Inguscio for making the optics for the Ti:sapphire ring laser available to us. Partial financial support from the European Commission under Contract No. CHRX-CT94-0464 is gratefully acknowledged.

*Present address: University of Toronto, Department of Physics, 60 St. George M5S-1A7 Toronto, Ontario, Canada.

†Present address: Centro Materiali Biofisica Medica, I-38050 Povo, Italy.

‡Also at Department of Chemical Engineering and Materials Science, University of Minnesota, Minneapolis, MN 55455, and Department of Physics, University of Trieste, I-34127 Trieste, Italy.

¹H. Haug and S. Schmitt-Rink, *J. Opt. Soc. Am. B* **2**, 1135 (1985).

²V. Pellegrini, F. Fuso, E. Arimondo, F. Castelli, L.A. Lugiato, G.P. Bava, and P. Debernardi, *Phys. Rev. A* **50**, 5219 (1994).

³G.P. Bava and L.A. Lugiato, *Opt. Commun.* **78**, 195 (1990).

⁴D.A.B. Miller, D.S. Chemla, T.C. Damen, A.C. Gossard, W. Wiegmann, T.H. Wood, and C.A. Burrus, *Appl. Phys. Lett.* **45**, 13 (1984).

⁵T. Rivera, F.R. Ladan, A. Izraël, R. Azoulay, R. Kuszelewicz, and J.L. Oudar, *Appl. Phys. Lett.* **64**, 869 (1994).

⁶R.D. Atanasov, F. Bassani, and V.M. Agranovich, *Phys. Rev. B* **50**, 7809 (1994).

⁷J. Kurgin, *Phys. Rev. B* **38**, 4056 (1988).

⁸E. Rosencher and Ph. Bois, *Phys. Rev. B* **44**, 11 315 (1991).

⁹C. Sirtori, F. Capasso, D.L. Sivco, S.N.G. Chu, and A.Y. Cho, *Appl. Phys. Lett.* **59**, 2302 (1991).

¹⁰Z. Xu, P.M. Fauchet, C.W. Rella, B.A. Richman, H.A. Schwettman, and G.W. Wicks, *Solid State Commun.* **93**, 903 (1995).

¹¹L. Tsang and S.L. Chuang, *Appl. Phys. Lett.* **62**, 2543 (1992).

¹²E. Rosencher, *J. Appl. Phys.* **73**, 1909 (1993).

¹³Y.L. Xie, Z.H. Chen, D.F. Cui, S.H. Pan, D.Q. Deng, Y.L. Zhou, H.B. Lu, Y. Huang, S.M. Feng, and G.Z. Yang, *Phys. Rev. B* **43**, 12 477 (1991).

¹⁴X.H. Qu, D.J. Bottomley, H. Ruda, and A.J. Springthorpe, *Phys. Rev. B* **50**, 5703 (1994).

¹⁵S. Scandolo, A. Baldereschi, and F. Capasso, *Appl. Phys. Lett.* **62**, 3138 (1993).

¹⁶S. Nakagawa, N. Yamada, N. Mikoshiba, and D.E. Mars, *Appl. Phys. Lett.* **66**, 2159 (1995).

¹⁷V. Pellegrini, R.D. Atanasov, A. Tredicucci, F. Beltram, C. Amzolini, L. Sorba, L. Vanzetti, and A. Franciosi, *Phys. Rev. B* **51**, 5171 (1995).

¹⁸F. Liaci, P. Bigenwald, O. Briot, B. Gil, N. Briot, T. Cloitre, and R.L. Aulombard, *Phys. Rev. B* **51**, 4699 (1995).

¹⁹V. Pellegrini, A. Tredicucci, F. Beltram, L. Vanzetti, M. Lazzarino, and A. Franciosi (unpublished).

²⁰H.P. Wagner, *Phys. Status Solidi B* **187**, 363 (1995).

²¹The frame of reference is taken with the *z* axis along the growth direction and the *x*, *y* axes rotated 45° in their plane with respect to the [010] and [001] directions.

²²R.D. Atanasov and F. Bassani, *Solid State Commun.* **84**, 71 (1992).

²³N. Bloembergen and P.S. Pershan, *Phys. Rev.* **128**, 193 (1962).

²⁴R.D. Atanasov, F. Bassani, and V.M. Agranovich, *Phys. Rev. B* **49**, 2658 (1994).

²⁵One should additionally consider that in the $\chi^{(2)}$ expression there are two terms, with opposite signs, involving transitions between two valence states and one conduction state and two conduction states and one valence state. In III-V lattice-matched materials these terms are similar and tend to cancel each other. In our system the mentioned similarity is broken by the strain-induced change in the lh confining potential.